**Supplemental Information**

K$^+$ Efflux-Independent NLRP3 Inflammasome

Activation by Small Molecules Targeting Mitochondria

Christina J. Groß, Ritu Mishra, Katharina S. Schneider, Guillaume Médard, Jennifer Wettmarshausen, Daniela C. Dittlein, Hexin Shi, Oliver Gorka, Paul-Albert Koenig, Stephan Fromm, Giovanni Magnani, Tamara Ćiković, Lara Hartjes, Joachim Smollich, Avril A.B. Robertson, Matthew A. Cooper, Marc Schmidt-Supprian, Michael Schuster, Kate Schroder, Petr Broz, Claudia Traidl-Hoffmann, Bruce Beutler, Bernhard Kuster, Jürgen Ruland, Sabine Schneider, Fabiana Perocchi, and Olaf Groß
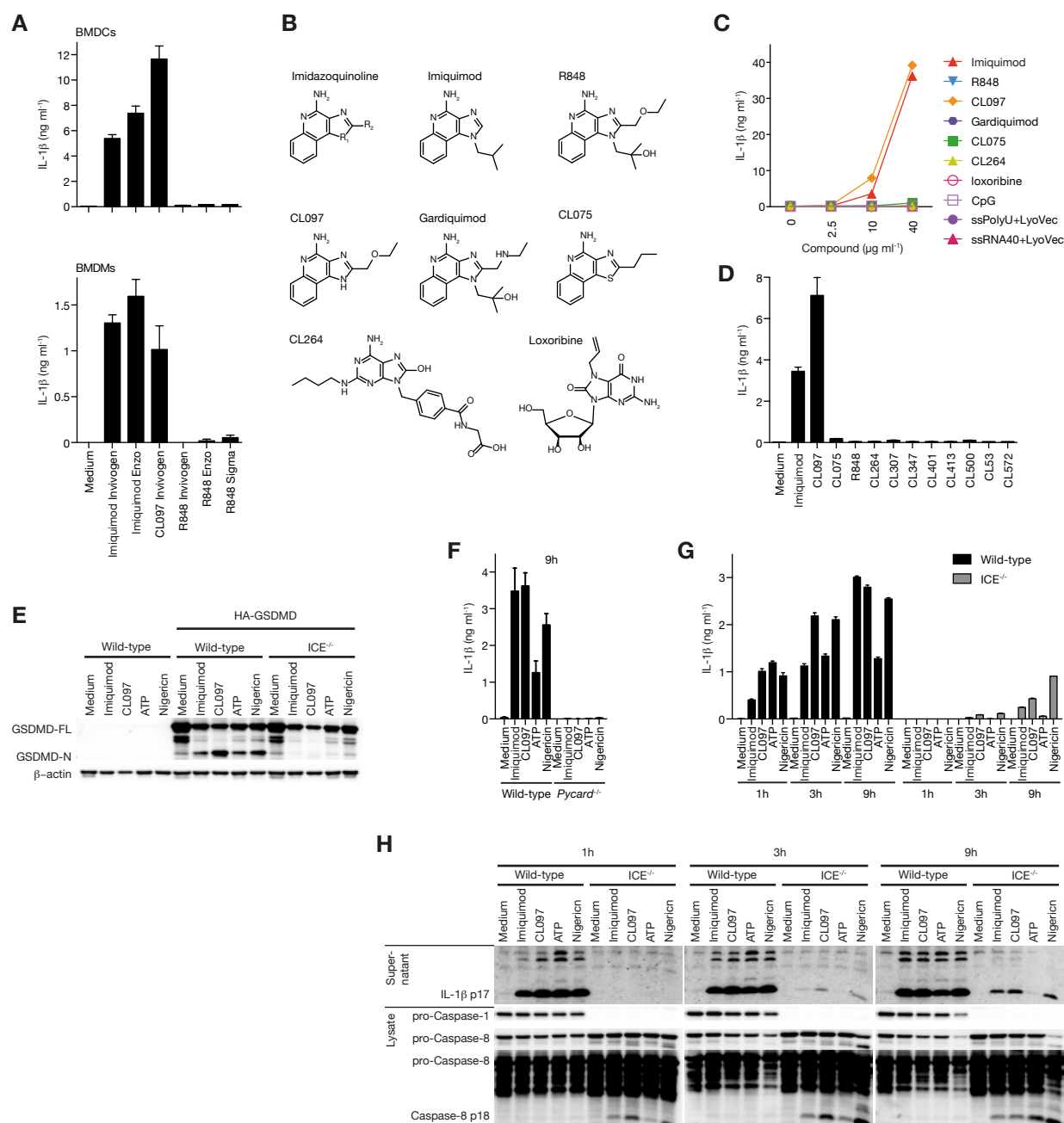
Figure S1. Supplemental data corresponding to main Figure 1: Imiquimod and CL097 are unique among TLR ligands in activating the NLRP3 inflammasome.

(A) LPS-primed BMDCs (top) or BMDMs (bottom) were stimulated with 15 µg ml^{-1} imiquimod, CL097, or R848 from different commercial sources. IL-1β release was quantified from cell-free supernatants by ELISA.

(B) Structures of selected imidazoquinolines and other TLR7/8 ligands used in this study.

(C, D) LPS-primed BMDCs were treated with increasing concentrations of imidazoquinoline or ssRNA ligands of TLR7/8 (C) or 16 µg ml^{-1} of the indicated TLR7/8 ligands from Invivogen (D). IL-1β secretion was quantified from cell-free supernatants by ELISA.

(E) Bone marrow cells from Caspase-1-deficient or wild-type mice were transduced with an N-terminally HA-tagged version of GSDMD or an empty vector control and differentiated into BMDMs. Cells were LPS-primed

and stimulated with inflammasome activators as indicated. Cell lysates were analyzed for the full-length and cleaved forms of GSDMD and for β-actin by immunoblotting.

(F, G) LPS-primed BMDCs from ASC- (*Pycard*, F) or Caspase-1- (G) deficient mice were treated with different NLRP3 inflammasome activators for prolonged periods as indicated. IL-1β secretion was quantified from cell-free supernatants by ELISA.

(H) Cell lysates and cell-free supernatants from (G) were subjected to immunoblotting and analyzed for the presence of the mature form of IL-1β in the supernatant (top) and for caspase-8 cleavage in cell lysates (bottom).

ELISA data are depicted as mean ± SEM of technical triplicates. The results from all experiments were verified on at least two or three separate occasions.
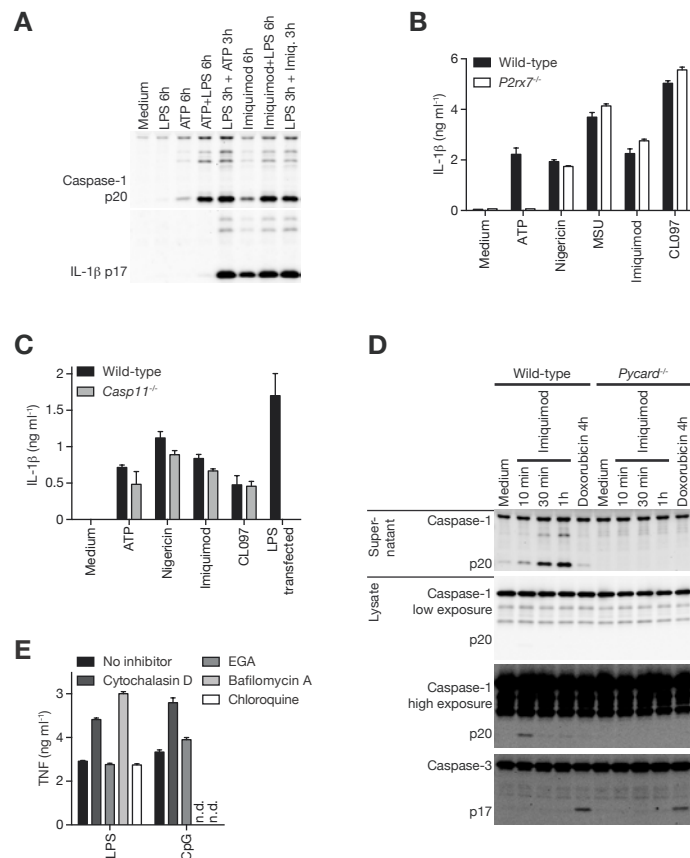
Figure S2. Supplemental data corresponding to main Figure 2: Imidazoquinolines do not require endosomal TLR signaling for NLRP3 activation.

(A) Unprimed BMDCs were treated with LPS, ATP, imiquimod or combinations thereof as indicated for a total of 6h. Cell-free supernatants were analyzed for the presence of the cleaved forms of caspase-1 (top) and IL-1β (bottom) by immunoblotting.

(B) LPS-primed BMDCs from wild-type or P2rx7-deficient mice were left untreated or stimulated as indicated. IL-1β was quantified from cell-free supernatants by ELISA.
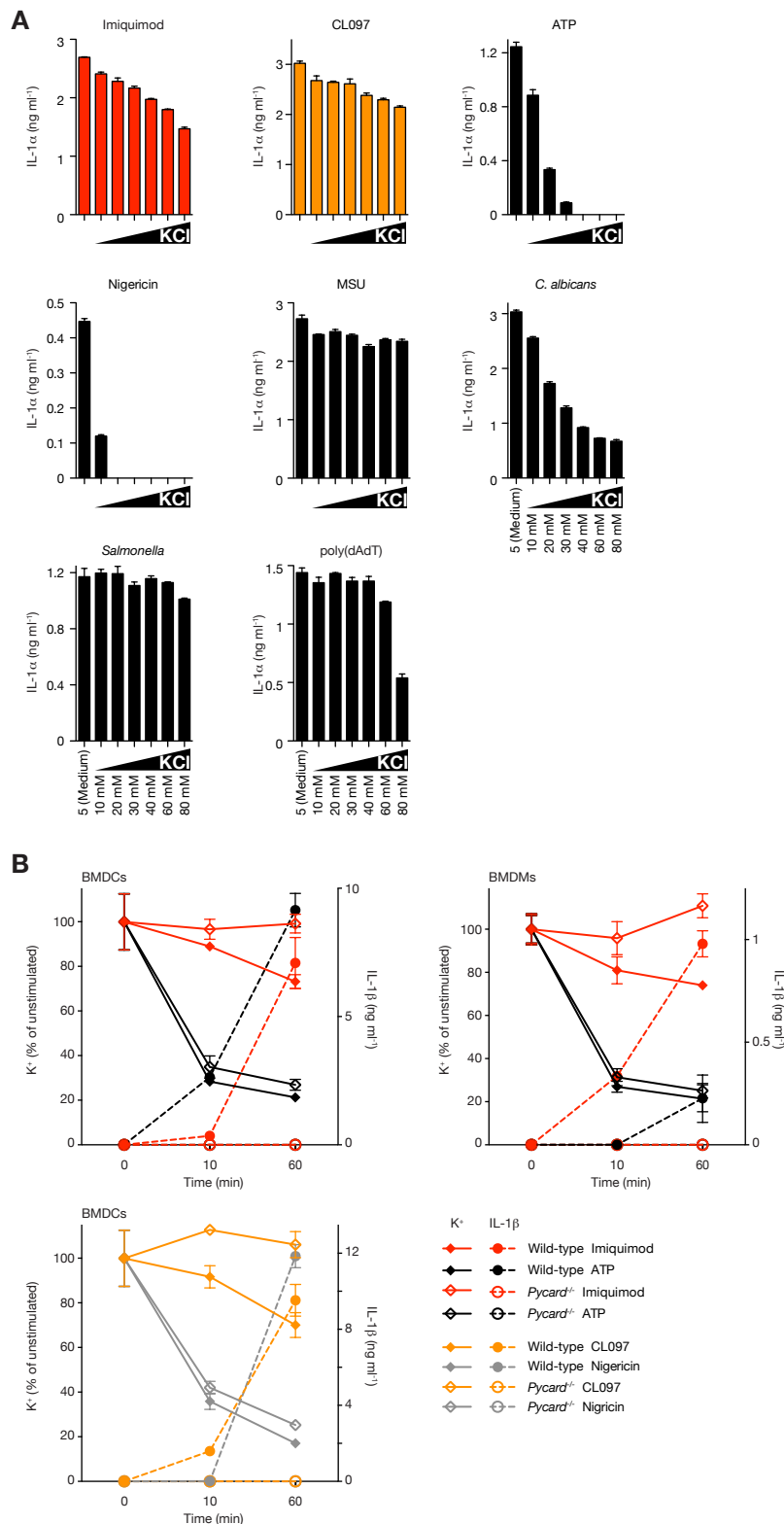
(C) BMDMs from wild-type or caspase-4/11-deficient mice primed with Pam3CSK4 in OptiMEM were left untreated or stimulated as indicated. IL-1β was quantified from cell-free supernatants by ELISA.
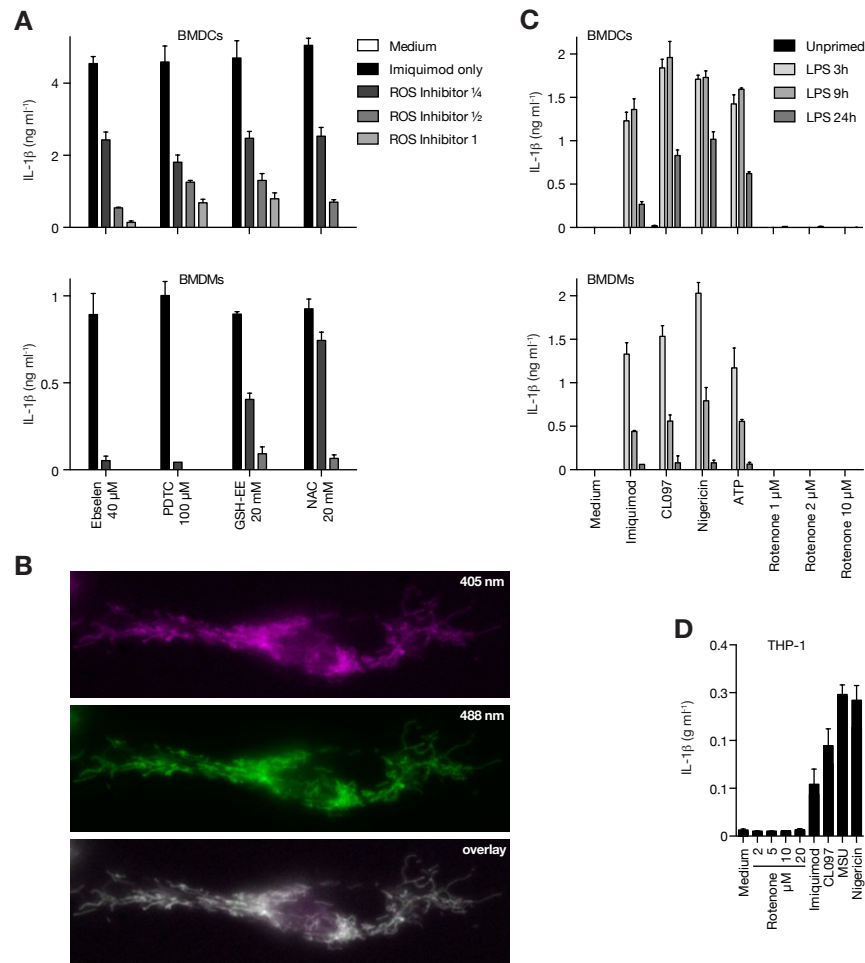
(D) LPS-primed BMDCs from wild-type or ASC (*Pycard*)-deficient mice were treated with imiquimod or doxorubicin for different time points. Caspase-1 release and cleavage from cell-free supernatants (top) and caspase-1 and caspase-3 cleavage in cell lysates were determined by immunoblotting.

(E) Corresponding to main Figure 2E: Unprimed BMDCs were treated with inhibitors of phagocytosis, endosomal trafficking, and lysosomal acidification 30 min prior to addition of LPS or the TLR9 ligand CpG ODN. TNF secretion was quantified from cell-free supernatants by ELISA.

ELISA data are depicted as mean ± SEM of technical triplicates. The results from all experiments were verified on at least two or three separate occasions.

Figure S3. Supplemental data corresponding to main Figure 3: K$^+$ efflux-independent NLRP3 inflammasome activation by imiquimod and CL097

(A) Corresponding to main Figure 3A: LPS-primed BMDCs were treated with increasing concentrations of extracellular KCl directly before stimulation with the indicated inflammasome activators. IL-1α secretion was quantified from cell-free supernatants by ELISA.

(B) LPS-primed wild-type or ASC (*Pycard*)-deficient BMDMs (left) or BMDCs (right) were left unstimulated (t=0) or stimulated with imiquimod (70 µM), CL097 (50 µM), ATP (5 mM), or nigericin (5 µM) for 10 or 60 minutes as indicated. K$^+$ efflux (left Y-axis, diamonds, solid lines) was determined from cell lysates prepared with HNO$_3$ containing vanadate as an internal standard by total reflection x-ray fluorescence analysis. IL-1β secretion (right Y-axis, circles, dashed lines) was quantified from cell-free supernatants by ELISA and is depicted as mean ± SEM of technical triplicates. The results from all experiments were verified on at least two or three separate occasions.

Figure S4. Supplemental data corresponding to main Figure 4: ROS is required for NLRP3 activation by imiquimod and CL097

(A) LPS-primed BMDCs (top) or BMDMs (bottom) were treated with increasing doses of ebselen, PDTC, GSH-EE or NAC for 30 min subsequently stimulated with imiquimod. The maximum dose of each inhibitor of a 1:1 dilution series is indicated. IL-1β was quantified from cell-free supernatants by ELISA.

(B) Corresponding to main Figure 5F, G, I: cells from CAR1 mice, transduced with an adenoviral construct encoding a mitochondrial matrix-targeted roGFP2 construct were analyzed by wide-field microscopy. Respective emission at 520 nm upon excitation at 405 and 488 nm is indicated.

(C) BMDCs (top) or BMDMs (bottom) were left unprimed or LPS-primed for 3h, 9h, and 24 and then stimulated with different inflammasome activators or different doses of rotenone as indicated. IL-1β secretion was quantified from cell-free supernatants by ELISA.

(D) Human THP-1 monocytes were PMA-primed and differentiated for 20h and stimulated with different inflammasome activators (120 μM imiquimod, 50 μM CL097, 400 μg ml^{-1} MSU, 5 μM nigericin) or different doses of rotenone as indicated. IL-1β secretion was quantified from cell-free supernatants by ELISA.

ELISA data are depicted as mean ± SEM of technical triplicates. The results from all experiments were verified on at least two separate occasions.
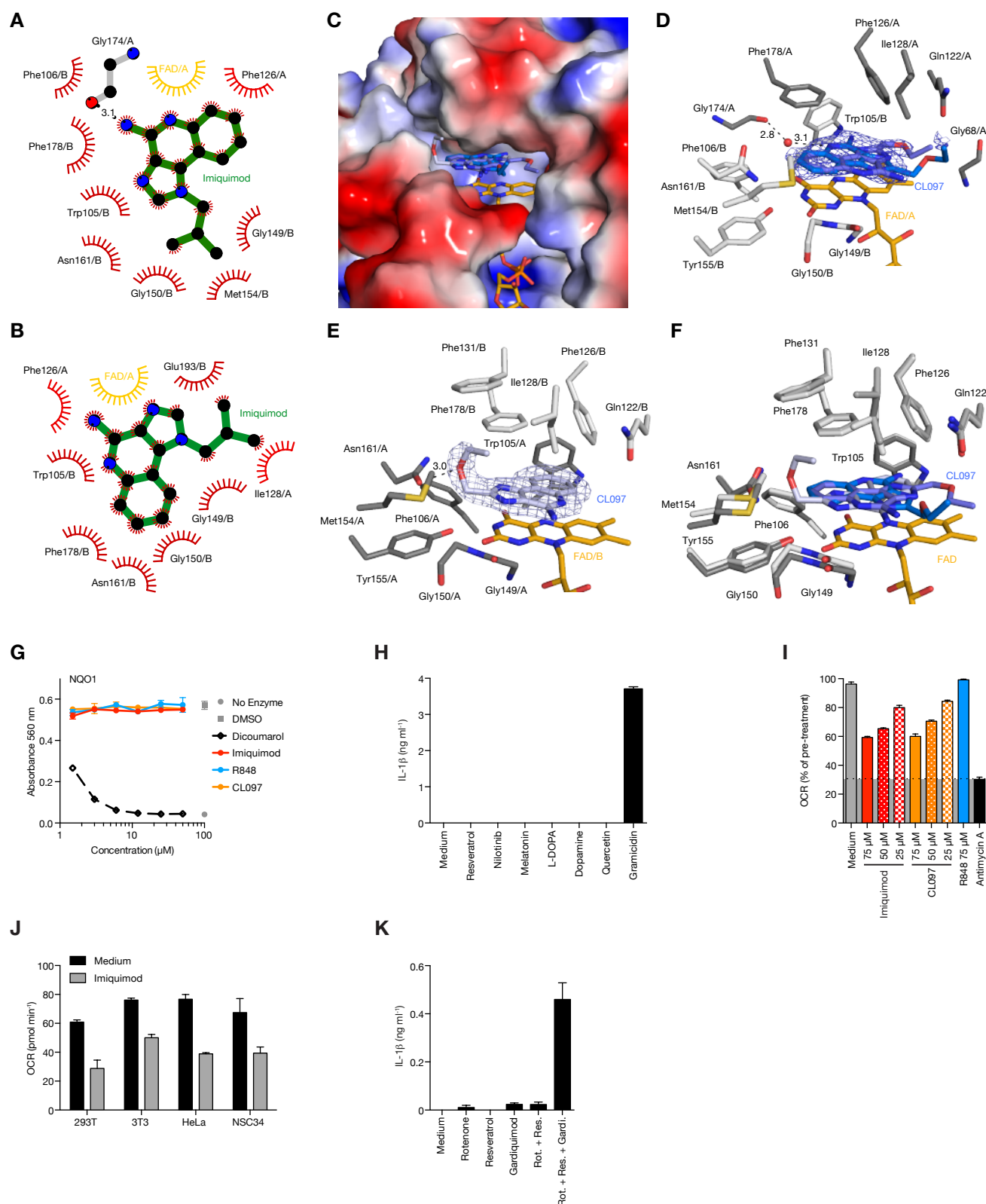
Figure S5. Supplemental data corresponding to main Figure 5: Imiquimod and CL097 inhibit the quinone oxidoreductases NQO2 and inhibit Complex I.

(A, B) Schematic representation of the interactions between NQO2 and imiquimod (green). Hydrophobic interactions are shown as half circles.

(C) Crystal structure of NQO2 in complex with CL097. Surface representation of the active site of NQO2 in complex with CL097.

(D, E) Unbiased Fo-DFc difference density, contoured at 2.5 σ prior to adding CL097 to the model coordinates, indicating possible alternative orientations. The residues of NQO2 lining the active side are shown as dark and light grey stick model (nitrogens are coloured blue, oxygens red, carbon atoms of amino acids grey, the FAD cofactor orange, CL097 blue, and hydrogen bonds are depicted as dashed lines).

(F) Superposition of both active side residues as in D, E, with the carbon atom of the different chains colored in light and dark grey, and CL097 (blue).

(G) Enzymatic activity of recombinant NQO1 in the presence of imidazoquinolines or the control inhibitor dicoumarol was determined by measuring the absorbance of reduced MTT.

(H) LPS-primed BMDCs were stimulated with the indicated NQO2 ligands (50 µM resveratrol, 25 µM nilotinib, 250 µM melatonin, 250 µM L-DOPA, 250 µM dopamine, 100 µM quercetin) or with gramicidin. IL-1β secretion was quantified from cell-free supernatants by ELISA.

(I) Oxygen consumption rate (OCR) of ASC-deficient BMDMs stimulated with increasing doses of imidazoquinolines or antimycin A (2 µM) for 7 min. The grey area of the graph below the level of antimycin A-treated samples is the level of non-mitochondrial respiration.

(J) Oxygen consumption rate (OCR) of four different cell lines, left untreated or stimulated with 75 µM imiquimod for 7 min.

(K) LPS-primed BMDCs were treated with the NQO2 inhibitor resveratrol (100 µM), the complex I inhibitor rotenone (2 µM) and the imidazoquinoline gardiquimod (75 µM) or combinations thereof as indicated. IL-1β secretion was quantified from cell-free supernatants by ELISA.

ELISA and OCR data are depicted as mean ± SEM of technical triplicates or quadruplicates. The results from all experiments were verified on at least two or three separate occasions.
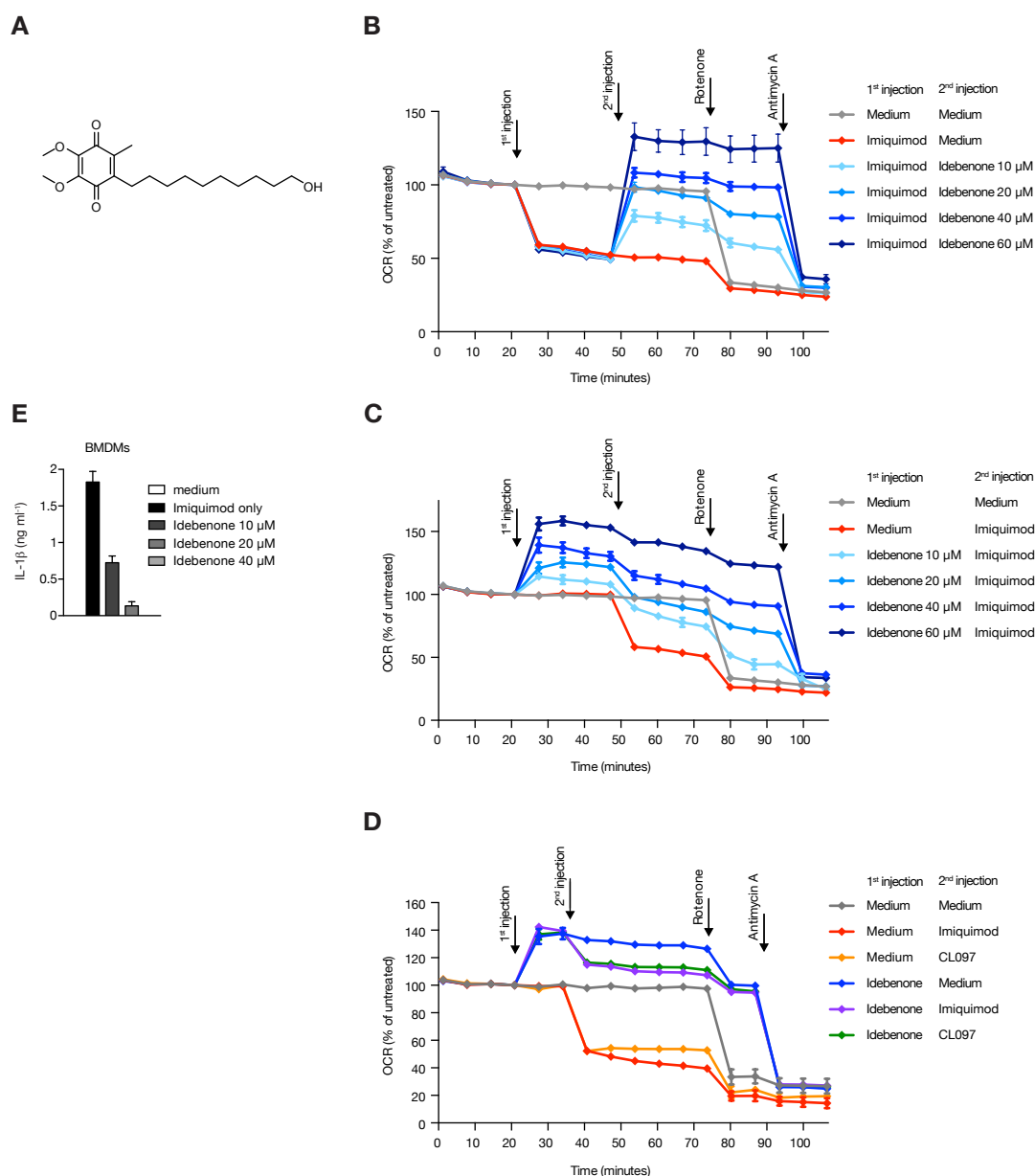
Figure S6. Supplemental data corresponding to main Figure 6: Elevation of Complex I dysfunction inhibits NLRP3 activation by imiquimod and CL097.

(A) Chemical structure of idebenone

(B, C) OCR of LPS-primed inflammasome-deficient BMDCs cells, either first treated with imiquimod (B, first arrow) and subsequently with four different doses of idebenone or first treated with four different doses of idebenone (C, first arrow) and then with imiquimod and subsequently with rotenone (2 µM) and finally with antimycin A (2 µM).

(D) OCR of LPS-primed inflammasome-deficient BMDCs, treated with idebenone and then with imiquimod or CL097 and subsequently with rotenone (2 µM) and finally with antimycin A (2 µM).

(E) LPS-primed BMDMs from wild-type mice were treated with increasing doses of idebenone for 30 min and subsequently stimulated with imiquimod as indicated. IL-1β was quantified from cell-free supernatants by ELISA.

ELISA and OCR data are depicted as mean ± SEM of technical triplicates or quadruplicates. The results from all experiments were verified on at least two or three separate occasions.

A

B

C
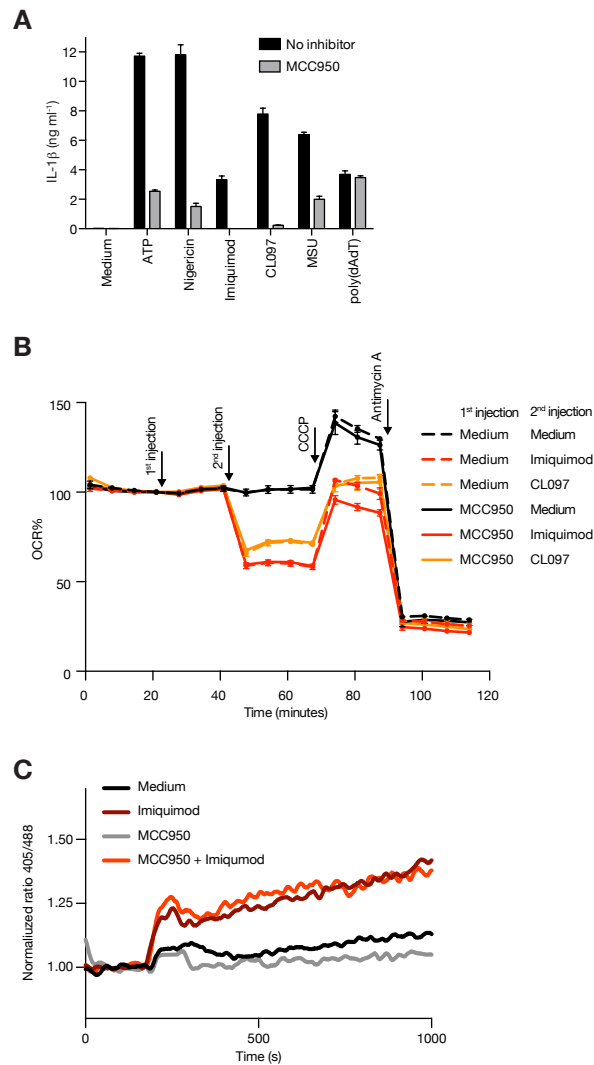
Figure S7. Additional data corresponding to main Figure 7: Imiquimod-induced NLRP3 activation requires NEK7 and is inhibited by MCC950

(A) LPS-primed wild-type BMDCs were treated with 1 µM MCC950 30 min prior to stimulation with various inflammasome activators as indicated. IL-1β secretion was quantified from cell-free supernatants by ELISA.

(B) OCR of LPS-primed inflammasome-deficient BMDCs, treated with MCC950 and then with imiquimod or CL097 and subsequently with rotenone (2 µM) and finally with antimycin A (2 µM).

(C) BMDMs from Vav-Cre - CAR1 mice, transduced with an adenoviral construct encoding a mitochondrial matrix-targeted roGFP2 construct were left untreated (black and dark-red line) or pre-treated with MCC950 (grey and light-red line) and monitored by flow cytometry. Upon base line determination for 200 seconds, cells were stimulated with 100 µM imiquimod (red lines) or medium (black and grey) and measurement was continued.

ELISA data are depicted as mean ± SEM of technical triplicates. The results from all experiments were verified on at least two or three separate occasions.

10

Table S1. Supplemental data corresponding to main Figure 5: Data collection and structure refinement statistics for crystal structure determination of NQO2. Statistics for the highest-resolution shell are shown in parentheses. Friedel mates were averaged when calculating reflection statistics.

	Imiquimod	CL097
Wavelength	0.976	0.976
Resolution range	44.4-1.75 (1.81-1.75)	44.3-1.65 (1.71-1.65)
Space group	P 2_1 2_1 2_1	P 2_1 2_1 2_1
Unit cell	57.7 80.9 106.2	57.7 80.9 106.2
Total reflections	224,722 (17,122)	200,332 (11,797)
Unique reflections	49,249 (2,863)	59,424 (5,486)
Multiplicity	4.6 (4.7)	3.4 (2.2)
Completeness (%)	0.93 (0.74)	0.99 (0.92)
Mean I/sigma(I)	6.01 (0.05)	9.42 (0.86)
Wilson B-factor	27.2	21.1
R-merge	0.124 (1.82)	0.069 (0.818)
R-meas	0.14 (2.05)	0.08 (1.04)
CC1/2	0.995 (0.749)	0.998 (0.544)
CC*	0.999 (0.925)	1 (0.84)
Reflections used in refinement	47,228 (2,802)	59,401 (5,484)
Reflections used for R-free	2,364 (142)	2,967 (273)
R-work	0.19 (0.395)	0.19 (0.379)
R-free	0.218 (0.378)	0.217 (0.367)
CC(work)	0.963 (0.785)	0.968 (0.661)
CC(free)	0.950 (0.749)	0.958 (0.765)
Number of non-hydrogen atoms	4,086	4,142
macromolecules	3,634	3,658
ligands	231	223
Protein residues	454	456
RMS(bonds)	0.960	0.958
RMS(angles)	1.72	1.41
Ramachandran favored (%)	97	97
Ramachandran allowed (%)	3.3	3
Ramachandran outliers (%)	0	0
Rotamer outliers (%)	0.77	0.76
Clashscore	2.26	1.45
Average B-factor	27.6	27.1
macromolecules	27.2	26.2
ligands	31.6	34.9
solvent	31.1	33.7
Number of TLS groups	18	

SUPPLEMENTAL EXPERIMENTAL PROCEDURES

Mice

Nlrp3$^{-/-}$ (Martinon et al., 2006), *Pycard*$^{-/-}$ (Mariathasan et al., 2006), ICE$^{-/-}$ (*Casp1/11*$^{-/-}$) (Kuida et al., 1995), *Il1b*$^{-/-}$, *Il1a*$^{-/-}$ (Horai et al., 1998), *TLR7*$^{-/-}$ (Hemmi et al., 2002), MyD88$^{-/-}$ (Adachi et al., 1998), P2rx7$^{-/-}$ (Solle et al., 2001), and CAR1 transgenic (Heger et al., 2015) mice on C57BL/6 background were housed under SOPF or SPF conditions at the Zentrum für Präklinische Forschung (Munich, Germany), Institut für Medizinische Mikrobiologie, Immunologie und Hygiene (Munich, Germany), Charles River Laboratories (Italy), or the Center of Infection and Immunity (University of Lausanne) in accordance with local and European guidelines. Bone marrow from *Nek7*$^{-/-}$ (Shi et al., 2016) and *Unc93b1*$^{3d/3d}$ (Tabeta et al., 2006) mice was obtained from Prof. Bruce Beutler and Dr. Philipp Yu, respectively.

Reagents

All tissue culture reagents were from Invitrogen, unless indicated otherwise. Imidazoquinolines and all other TLR ligands were from Invivogen, unless indicated otherwise. MCC950 was synthesized as previously reported (Coll et al., 2015). All other chemicals and reagents were from Sigma, unless indicated otherwise. MSU crystals were prepared as previously described (Martinon et al., 2006). Preparation of and stimulation with *C. albicans* and *Salmonella* was performed as previously described (Groß et al., 2012).

BMDC and BMDM Preparation and Stimulation

Cells were cultured at 37°C/5% CO$_2$ in a humidified incubator unless indicated otherwise. Murine bone marrow-derived dendritic cells (BMDCs) and bone marrow-derived macrophages (BMDMs) were differentiated from tibial and femoral bone marrow aspirates as previously described in detail (Schneider et al., 2013). Recombinant murine M-CSF (for BMDMs) and GM-CSF (for BMDCs) were both from Immunotools and were used at 20 ng ml^{-1}. After 6-8 days of differentiation, cells were plated in 96-well plates at a density of 0.12-0.15x10^6 cells/well, primed with 20 ng ml^{-1} *E. coli* K12 ultra-pure LPS for 3h and treated with inflammasome activators for 0.5-6h. All stimulations were performed in triplicate and cytokine production in cell-free supernatants was measured by ELISA. Typical stimulus concentrations for TLR ligands used for priming or TNF production (2.5-4h stimulation) were: 20-100 ng ml^{-1} LPS, 2 µg ml^{-1} R848, 10 µg ml^{-1} CpG DNA, 5 µg ml^{-1} PGN, 2 µg ml^{-1} Pam3CSK4. Typical inflammasome activator concentrations and times were as follows: 5 mM ATP 30 min, 5 µM nigericin 30-45 min, MOI 5 *C. albicans* 4 h, 300 µg ml^{-1} MSU/Alum/Silica for 4h, 2 µg ml^{-1} poly(dA:dT) 2-3h (transfected with Lipofectamine 2000, Invitrogen), MOI 20 Salmonella 1-2h. Imiquimod and CL097 were used at 15-20 µg ml^{-1} or 70 µM for 1-2h for inflammasome activation, though inflammasome activation can be observed as early as 10 min after stimulation with these compounds. Inhibitors were added after 2.5-3h of priming, and 20-30 min before stimulation with inflammasome activators. Inhibitor concentrations were as follows, unless indicated otherwise: 20 µM zVAD-fmk (Enzo), 20 µM Ac-YVAD-cmk (Enzo), 30 µM ebselen (Enzo), 50 µM ammonium pyrrolidinedithiocarbamate (PDTC), 20 mM GSH-EE, 20 mM N-acetyl-L-cysteine (NAC), 30 µM idebenone, 5 µM MCC950. To minimize off-target effects of extracellular KCl, it was added and mixed well by careful pipetting immediately before addition of inflammasome activators. All inflammasome activators were carefully titrated and used at the lowest dose and the shortest time required to cause significant IL-1 secretion. Inhibitors were also titrated, and the lowest effective dose was used.

Immunodetection of Proteins

For cytokine quantification of cell-free supernatants, ELISA kits for murine IL-1α, IL-1β, and TNF from eBioscience were used according to manufacturer's instructions. ELISA data is depicted as mean ± SEM of technical triplicates. For immunoblot analysis of cell-free supernatant and cell lysates prepared in SDS- and DTT-containing sample buffer, triplicate samples were pooled and proteins were separated by SDS-PAGE and transferred to nitrocellulose using standard techniques (Schneider et al., 2013). To analyze inflammasome formation, the insoluble fraction of NP-40-lysed cells was left untreated or cross-linked with disuccinimidyl suberate (Thermo Scientific) before immunoblot analysis, as previously described (Fernandes-Alnemri et al., 2007). Primary antibodies were as follows: goat anti-mouse IL-1β (AF-401, R&D Systems), mouse anti-mouse caspase-1 p20 (Casper-1, Adipogen), hamster anti-mouse IL-1α (ALF-161, eBioscience), mouse anti-mouse NLRP3 (Cryo-2, Adipogen), rabbit anti-ASC (AL177, Adipogen), anti-mouse caspase-8 (1G12, Enzo), rabbit anti-caspase-3 (9662 Cell Signaling), and anti-NEK7 (EPR4900, Abcam).

Fluorescence Imaging

For immunofluorescence imaging of ASC specks, murine BMDCs were seeded at 8×10^5 cells/well in 8-chamber culture slides (Falcon). Cells were primed with 50 ng ml^{-1} of LPS for 2h followed by a treatment with imiquimod (100 µM for 1.5 h), nigericin (10 µM for 45 mins) or left untreated. After treatments, cells were washed with PBS, fixed in 4% paraformaldehyde for 10 min and extracted in PBS with 0.1% (v/v) Triton-X100 for 5 min. Cells were stained with anti-ASC antibody (AL177, Adipogen) diluted in blocking buffer consisting of PBS, 5% FCS and 0.1% Triton X-100, followed by an anti-rabbit secondary and finally mounted in Vectashield containing DAPI (Vector Laboratories). Confocal microscopy of immunostained cells was performed with a Leica SP8 confocal microscope equipped with a 63×/1.40 oil objective (Leica Microsystems) keeping the laser settings of images constant for comparison.

Retroviral transduction

HEK293T cells were transfected with GSDMD-HA-Flag-pMIP, gag-pol, and VSV-G envelope using TurboFect (Thermo). Supernatant containing the viral particles was harvested 48h after transfection and filtered (0.45 µm). Polybrene was added to a final concentration of 4 µg ml^{-1}. Day 1 BMDMs were mixed with viral supernatant, and spun in 6-well plates for 2h at 32°C, 1000 xg. The transduction was repeated after 24 hours with fresh virus. Transduced BMDMs were harvested on day 8.

Generation of mutant HoxB8 cells using CRISPR/Cas9 technology

Conditionally immortalized myeloid progenitor cells ('HoxB8 cells') were generated and cultured as described before (Wang et al., 2006) by transducing bone marrow from a C57BL/6 mouse with a retrovirus containing ER-HoxB8 in the presence of estrogen and GM-CSF. SpCas9-2A-GFP from pSpCas9(BB)-2A-GFP (pX458, Addgene plasmid # 48138, a gift from Feng Zhang (Ran et al., 2013)) was cloned into pMIG and then introduced into HoxB8 cells by retroviral transduction. Cas9-expressing HoxB8 cells ('Cas9-HoxB8 cells') were obtained by sorting for cells with high GFP expression. sgRNAs were cloned as described (Ran et al., 2013) into a pMSCVpuro-based plasmid coding for the expression cassette for an sgRNA under the U6 promoter (pMSCV-sgRNA) derived from pX458. Mutant HoxB8 cells were made by introducing individual sgRNAs with retroviral transduction into Cas9-HoxB8 cells followed by selection in medium containing 5 µg ml^{-1} Puromycin. We used the same sgRNA sequences as in the Brie library (Doench et al., 2016), except for Gsdmd_5, which was selected using the benchling tool (benchling.com) and GFP_1 to GFP_5, which were selected using the CHOPCHOP tool (Montague et al., 2014). The specific sgRNA target sequences are:

Gsdmd_1:   5'-AGGTTGACACATGAATAACG-3'
Gsdmd_2:   5'-CAGTATACACACATTCATGG-3'
Casp1_1:   5'-GAGGGCAAGACGTGTACGAG-3'
Casp1_2:   5'-AAACATTACTGCTATGGACA-3'
GFP_1:   5'-GGGCGAGGAGCTGTTCACCG-3'
GFP_2:   5'-GGTCAGGGTGGTCACGAGGG-3'

For stimulation assays, HoxB8 cells were differentiated for 6 days by withdrawing estrogen from the culture medium (Wang et al., 2006).

Flow Cytometric Analysis of Endolysosomal Leakage

ASC-deficient BMDMs were incubated for 30 min with acridine orange (1 µg ml^{-1}), washed three times in phenol red-free HBSS with 5mM EDTA and 3% FCS. After a constant baseline was obtained by flow cytometry, the stimulation of cells with imiquimod, R848, CL097 and gardiquimod (100 µM) was followed as a time course for 1h at 37°C. Maximum endolysosomal rupture was confirmed by addition of LLOMe (1 µM) in the last 10 min. Endolysosomal leakage was assessed by a ratiometric measurement of the change in distribution of the dye in the acidic endolysosomal compartment (red, on PerCP channel) and the cytoplasmic/nuclear compartment (green, on FITC channel). A FACS Aria III (BD Biosciences) flow cytometrer was used. Data were acquired with DIVA (BD Biosciences) and were analyzed with FlowJo software.

K$^+$ Measurement

Intracellular K$^+$ measurements were performed using an ion-selective electrode (ISE) (Cobas analyzer, Roche). Cells were dislodged and 10^7 cells per condition were stimulated in suspension. After the intended duration, cells were immediately transferred to ice and pelleted by centrifugation at 400xg for 5 min at 4°C in

15 ml conical tubes. Medium was carefully and completely removed and subjected to IL-1β measurement by ELISA. The cell pellet was suspended in 150 µl of ultrapure water and cellular content was released by repeated freeze-thaw cycles in liquid nitrogen. Debris was pelleted by centrifugation at 14000 xg for 10 min at 4°C and 100 µl of the clarified lysate was subjected to K$^+$ measurement.

Alternatively, total reflection x-ray fluorescence analysis (TXRF) was used, providing high absolute detection power (usually in the lower pg range) which in turn dramatically reduces the required sample volume. Cells were stimulated as usual in 96-well plates. After supernatants were removed for ELISA or immunoblot analysis of inflammasome activation, the residual medium was carefully but completely aspirated. The cells were extracted by adding 25 µl 3% dilution of ultra-pure HNO3 containing 5 µg ml^{-1} vanadium as internal standard into the wells. 5 µL of the lysates were spotted on a silicon wafer and evaporated to dryness. Measurement was performed with an Atomika TXRF 8010 device equipped with a molybdenum x-ray tube. Due to a sophisticated geometry, the monochromatized x-ray beam strikes the ultra-planar and smooth surface of the silicon wafer at a very small glancing angle (< 0,1°) and is totally reflected. Both, the incident and the reflected beam intensively excite the sample spotted on the wafer (area of excitation is approx. 1 cm^2). The sample then emits element characteristic X-ray fluorescence radiation, which is detected by a liquid nitrogen cooled semiconductor detector arranged perpendicular to the sample. Characteristic signals for potassium (E_{K_α} = 3,31 keV) and vanadium (E_{K_α} = 4,95 keV) were used for data evaluation using the software Spectra Picofox (Bruker, Berlin, Germany).

Metabolic Analysis

Oxygen consumption rate (OCR) was measured using a Seahorse XF96 Extracellular Flux Analyzer (Agilent). BMDMs or BMDCs (6-8x10^4/well in quadruplicates) were seeded the evening before the experiment in 96-well plates. The morning of the experiment the cells were primed with 50 ng ml^{-1} LPS for 2-3h before the medium was changed to bicarbonate- and phenol red-free DMEM 5030 (Sigma) containing 20 ng ml^{-1} recombinant murine M-CSF or GM-CSF, 10 mM glucose, and 2 mM glutamine. The cells were then incubated for at least 1h at 37°C in a non-CO$_2$ incubator. To avoid respiratory chain inhibition that occurs after 8h of stimulation with TLR ligands, the time between LPS addition and the beginning of the experiment did not exceed 4h (Everts et al., 2012). For analysis of intact cells, mix-wait-measure times 1 min – 2 min – 3 min were used, and stimuli were injected via ports. Imidazoquinolines were used at 70 µM (=20 µg ml^{-1} for imiquimod) unless indicated otherwise. Respiratory chain inhibitors were used at the following concentrations: 0.5 µM CCCP, 3.5 µM oligomycin A, 2 µM antimycin A. The protocol for OCR measurements of HEK293T human embryonic kidney cells, 3T3 murine fibroblasts, HeLa human epithelial cells, NSC34 mouse motor neuron-like cells, human primary keratinocytes, and HaCaT immortalized human keratinocytes was the same except assay medium did not contain growth factors and cells were not LPS-treated. Cell lines were cultivated in DMEM with 10% FCS, 100 U ml^{-1} penicillin, and 100 mg ml^{-1} streptomycin, 2 mM glutamine, and 10 mM glucose using standard protocols.

To analyze the activity of individual respiratory chain complexes, BMDMs were permeabilized for 5 min in MAS buffer (220 mM mannitol, 70 mM sucrose, 10 mM KH$_2$PO$_4$, 5 mM MgCl$_2$, 2 mM HEPES, 1 mM EGTA, 0.4% fatty acid-free BSA pH 7.2) containing 40 µM digitonin. Digitonin-containing medium was removed and replaced with MAS buffer containing 2 mM ADP along with combinations of TCA cycle intermediates and electron donors at the following concentrations: 10 mM succinate, 2 mM malate, 5 mM pyruvate, 5 mM glutamate, 2 µM rotenone, 0.5 mM *N,N,N',N'*-tetramethyl-*p*-phenylenediamine (TMPD), 2 mM ascorbate (Salabei et al., 2014). Stimuli were added directly to the assay medium before measurement began. For analysis of permeabilized cells, mix-wait-measure times of 1 min – 10 s – 2.5 min were used, without initial equilibration. Intracellular ATP was quantified using the CellTiterGlo Assay (Promega) according to the manufacturers instructions. NAD$^+$/NADH ratios were measured by enzymatic cycling using the NAD$^+$/NADH Quantification kit (Biovision).

Measurement of ROS and roGFP2 oxidation

ASC-deficient BMDMs were stimulated for 1h with imidazoquinoliones or rotenone (2 µM), or left untreated. Following stimulation, cells were stained with CellROX or MitoSOX for 10 min in accordance with the manufacturer's instructions (Thermo Fisher). ROS signal was measured with a FACS Canto (BD Biosciences) and analyzed using FlowJo software.
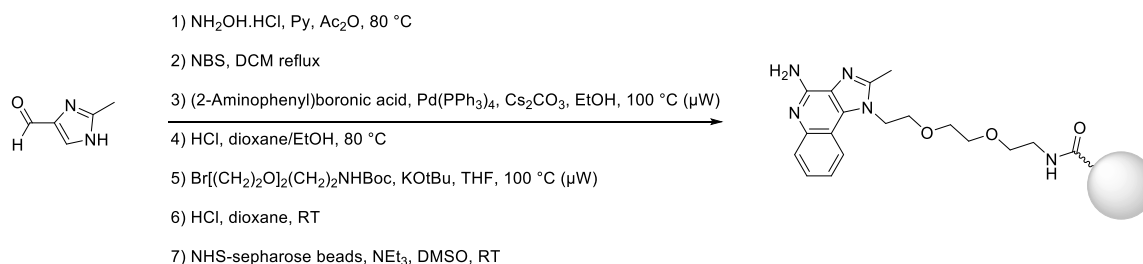
BMDMs from CAR1 transgenic mice (Heger et al., 2015) were transduced for 24h with Ad5 adenovirus (MOI 50) encoding redox sensing roGFP2 constructs targeted to the mitochondrial matrix (mito-roGFP) or untargeted that localizes in the cytosol (cyto-roGFP) (ViraQuest Inc., North Liberty, Iowa). Viral titer was

determined using the Adeno-X Rapid Titer Kit (Takara-Clontech). After baseline acquisition, real-time change in redox potential of mito- or cyto-roGFP expressing BMDMs subsequent to stimulation with imiquimod, R848 (100 μM), or rotenone (2 μM) was followed by flow cytometry for 20 min at 37°C in FACS buffer. Redox change was expressed by a ratiometric readout of the change in emission intensities of roGFP2 at 520 nm when exited at 405 or 488 nm, where an increase in the 405:488 ratio indicates roGFP2 oxidation. FACS Aria III (BD Biosciences) flow cytometer was used. Data were acquired with DIVA (BD Biosciences) and were analyzed with FlowJo software. For inhibitor studies, ebselen (20 μM) or PDTC (100 μM) was applied to the cells 20 minutes prior to stimulation and left in the buffer during measurement.

Chemical Proteomics

The imidazoquinoline affinity matrix was prepared in seven steps inspired by Ferguson's retrosynthetic disconnection(Shi et al., 2012), starting from 2-methyl-1H-imidazole-4-carbaldehyde. The aldehyde was converted into a nitrile (Kawakami et al., 2003), the 5-position brominated with NBS for further Suzuki coupling with (2-aminophenyl)boronic acid. HCl could then help cyclise the di-aryl into the tricyclic amine pharmacophore, onto which was appended the boc-protected amino ethylene glycol linker, which, once deprotected, was instrumental for the immobilisation on the solid matrix at a concentration of 2 μmol / mL beads (Médard et al., 2015).

1) $NH_2OH.HCl$, Py, Ac_2O, 80 °C

2) NBS, DCM reflux

3) (2-Aminophenyl)boronic acid, $Pd(PPh_3)_4$, Cs_2CO_3, EtOH, 100 °C (μW)

4) HCl, dioxane/EtOH, 80 °C

5) $Br[(CH_2)_2O]_2(CH_2)_2NHBoc$, KOtBu, THF, 100 °C (μW)

6) HCl, dioxane, RT

7) NHS-sepharose beads, NEt_3, DMSO, RT

The competitive pulldown assay was conducted in a 96 well plate format as reported previously when using Kinobeads, using the imidazoquinoline affinity matrix (35 μL beads per pulldown), BMDC lysate (3.1 mg total protein per pulldown) and a dilution series of imiquimod (DMSO, 30 nM, 100 nM, 300 nM, 1 μM, 3 μM, 10 μM, 30 μM and 100 μM). Mass spectrometry readout and data analysis were carried on an Orbitrap QExactive and MaxQuant (version 1.4.0.5) using the Uniprot mouse reference database (v06.06.14) as previously detailed. Dose-response curves generated using a R script were visually inspected.

Cloning, protein expression and purification of NQO2

For expression the codon-optimised, full-length DNA sequence (Thermo Fisher) coding for the human NQO2 enzyme, which shares 81% and 91% sequence identity and similarity, respectively, with the mouse homologue, was cloned in frame with a C-terminal His$_6$-affinity tag into the expression plasmid pET28. The expression plasmid was transformed in *Escherichia coli* BL21 (DE3) (Novagen) and the cells grown in 2YT medium supplemented with 50 μg ml^{-1} kanamycin at 37 °C until an optical density of 1 was reached. Protein expression was induced by adding 1 mM isopropyl-β-D- thiogalactoside (IPTG) and continued at 30 °C over night. Cells were harvested by centrifugation, resuspended in 50 mM Tris-HCl, pH 7.4, 300 mM NaCl, 10 mM imidazole (lysis buffer) supplemented with complete protease inhibitor cocktail (Roche) and lysed by sonication. Protein purification was carried out by Ni-affinity chromatography (Ni-NTA superflow, Qiagen). The protein buffer was exchanged to 50 mM Tris-HCl, pH 8, the protein concentrated to 50 mg ml^{-1} using centrifugal filter devices (Amicon Ultra Centrifugal Filter Device, Millipore), aliquoted and stored at -80 °C until further use.

NQO1 and NQO2 enzymatic activity assays

Inhibition of NQO1 and NQO2 enzymatic activity was determined as previously described, with some modifications (2014). Recombinant NQO2 was prepared as described above and recombinant NQO1 was from Sigma. Assay buffer (50 mM Hepes-KOH, pH 7.4, with 0.01% Tween20, 0.18 mg ml^{-1} BSA, and 1 μM FAD) with varying concentrations of test compounds was mixed 1:1 with 50 μl enzyme buffer (assay buffer with 50 ng of recombinant NQO1 or 20 ng NQO2 per well) and rested for 5 min at room temperature. Enzymatic reactions were initiated by adding 50 μl of detection buffer (assay buffer containing 500 μM NADH (for NQO1) or 100 μM of 1-benzyl-1,4-dihydronictinamide BNAH (for NQO2) as co-substrates along with 600

µM MTT and 300 µM menadione). Absorbance of the samples was measured after 2 min at 560 nm using a plate reader.

Crystallization and structure determination of NQO2

For co-crystallization human NQO2 in 50 mM Tris-HCl, pH 8, 10 µM flavin adenine dinucleotide, 1 mM dithiothreitol were mixed with imiquimod or CL097 (4 mM stock solution in dimethyl sulfoxide) to a final concentration of 7.5 mg ml^{-1} NQO2 and 100 µM of the inhibitor prior to crystallization. Crystals were grown in 0.1 M Tris-HCl, pH 8.5, 2 M ammonium sulfate, at 20 °C. Data collection was carried out at the PXI beamline, Swiss Light Source (SLS) Villigen Switzerland and ID23-2 beamline, European Synchrotron Radiation Facility (ESRF), Grenoble, France. Diffraction data were processed to 1.75 Å (imiquimod) and 1.65 Å (CL097), respectively, with XDS (Kabsch, 2010) and belonged to the space group P212121. The resolution cut-offs were chosen using the correlation coefficient of random half-data sets (1/2 CC) of about 50% (Diederichs and Karplus, 2013; Evans, 2012; Karplus and Diederichs, 2012). For all data sets the same set of FreeR-reflections was used. The structures were solved by placing the coordinates of human NQO2 (PDB code 2BZS) in the asymmetric crystal unit using rigid-body refinement, followed by restrained refinement in REFMAC5 (Murshudov et al., 2011). Peaks for imiquimod and CL097 were visible in the corresponding, unbiased difference density maps (Figure 4C and S4D, E). Iterative cycles of manual building and refinement were carried out in COOT (Emsley et al., 2010) and REFMAC5. Restraints and number of TLS groups were optimised using the PDB Redo server (Joosten et al., 2014). For data processing and structure refinement statistics see Table S1. Structural superpositions were done with SSM (Krissinel and Henrick, 2004) and interactions analysed by LIGPLOT (Wallace et al., 1995). All structural figures were prepared with PyMol (Delano Scientific).

SUPPLEMENTAL REFERENCES

Adachi, O., Kawai, T., Takeda, K., Matsumoto, M., Tsutsui, H., Sakagami, M., Nakanishi, K., and Akira, S. (1998). Targeted disruption of the MyD88 gene results in loss of IL-1- and IL-18-mediated function. Immunity *9*, 143–150.

Coll, R.C., Robertson, A.A.B., Chae, J.J., Higgins, S.C., Muñoz-Planillo, R., Inserra, M.C., Vetter, I., Dungan, L.S., Monks, B.G., Stutz, A., et al. (2015). A small-molecule inhibitor of the NLRP3 inflammasome for the treatment of inflammatory diseases. Nature Medicine *21*, 248–255.

Diederichs, K., and Karplus, P.A. (2013). Better models by discarding data? Acta Crystallogr. D Biol. Crystallogr. *69*, 1215–1222.

Doench, J.G., Fusi, N., Sullender, M., Hegde, M., Vaimberg, E.W., Donovan, K.F., Smith, I., Tothova, Z., Wilen, C., Orchard, R., et al. (2016). Optimized sgRNA design to maximize activity and minimize off-target effects of CRISPR-Cas9. Nature Biotechnology *34*, 184–191.

Emsley, P., Lohkamp, B., Scott, W.G., and Cowtan, K. (2010). Features and development of Coot. Acta Crystallogr. D Biol. Crystallogr. *66*, 486–501.

Evans, P. (2012). Resolving Some Old Problems in Protein Crystallography. Science *336*, 986–987.

Everts, B., Amiel, E., van der Windt, G.J.W., Freitas, T.C., Chott, R., Yarasheski, K.E., Pearce, E.L., and Pearce, E.J. (2012). Commitment to glycolysis sustains survival of NO-producing inflammatory dendritic cells. Blood *120*, 1422–1431.

Fernandes-Alnemri, T., Wu, J., Yu, J.-W., Datta, P., Miller, B., Jankowski, W., Rosenberg, S., Zhang, J., and Alnemri, E.S. (2007). The pyroptosome: a supramolecular assembly of ASC dimers mediating inflammatory cell death via caspase-1 activation. Cell Death Differ *14*, 1590–1604.

Groß, O., Yazdi, A.S., Thomas, C.J., Masin, M., Heinz, L.X., Guarda, G., Quadroni, M., Drexler, S.K., and Tschopp, J. (2012). Inflammasome activators induce interleukin-1α secretion via distinct pathways with differential requirement for the protease function of caspase-1. Immunity *36*, 388–400.

Heger, K., Kober, M., Rieß, D., Drees, C., de Vries, I., Bertossi, A., Roers, A., Sixt, M., and Schmidt-Supprian, M. (2015). A novel Cre

recombinase reporter mouse strain facilitates selective and efficient infection of primary immune cells with adenoviral vectors. Eur. J. Immunol. *45*, 1614–1620.

Hemmi, H., Kaisho, T., Takeuchi, O., Sato, S., Sanjo, H., Hoshino, K., Horiuchi, T., Tomizawa, H., Takeda, K., and Akira, S. (2002). Small anti-viral compounds activate immune cells via the TLR7 MyD88-dependent signaling pathway. Nat Immunol *3*, 196–200.

Horai, R., Asano, M., Sudo, K., Kanuka, H., Suzuki, M., Nishihara, M., Takahashi, M., and Iwakura, Y. (1998). Production of mice deficient in genes for interleukin (IL)-1 alpha, IL-1 beta, IL-1 alpha/beta, and IL-1 receptor antagonist shows that IL-1 beta is crucial in turpentine-induced fever development and glucocorticoid secretion. Journal of Experimental Medicine *187*, 1463–1475.

Joosten, R.P., Long, F., Murshudov, G.N., and Perrakis, A. (2014). The PDB_REDO server for macromolecular structure model optimization. IUCrJ *1*, 213–220.

Kabsch, W. (2010). Integration, scaling, space-group assignment and post-refinement. Acta Crystallogr. D Biol. Crystallogr. *66*, 133–144.

Karplus, P.A., and Diederichs, K. (2012). Linking Crystallographic Model and Data Quality. Science *336*, 1030–1033.

Kawakami, J., Kimura, K., and Yamaoka, M. (2003). A convenient synthesis of 4(5)-alkylacyl-1H-imidazoles from 4(5)-imidazolecarboxaldehyde. Synthesis-Stuttgart 677–680.

Krissinel, E., and Henrick, K. (2004). Secondary-structure matching (SSM), a new tool for fast protein structure alignment in three dimensions. Acta Crystallogr. D Biol. Crystallogr. *60*, 2256–2268.

Kuida, K., Lippke, J.A., Ku, G., Harding, M.W., Livingston, D.J., Su, M., and Flavell, R.A. (1995). Altered Cytokine Export and Apoptosis in Mice Deficient in Interleukin-1-Beta Converting-Enzyme. Science *267*, 2000–2003.

Mariathasan, S., Weiss, D.S., Newton, K., McBride, J., O'Rourke, K., Roose-Girma, M., Lee, W.P., Weinrauch, Y., Monack, D.M., and Dixit, V.M. (2006). Cryopyrin activates the inflammasome in response to toxins and ATP. Nature *440*, 228–232.

Martinon, F., Pétrilli, V., Mayor, A., Tardivel, A., and Tschopp, J. (2006). Gout-associated uric acid crystals activate the NALP3 inflammasome. Nature *440*, 237–241.

Médard, G., Pachl, F., Ruprecht, B., Klaeger, S., Heinzlmeir, S., Helm, D., Qiao, H., Ku, X., Wilhelm, M., Kuehne, T., et al. (2015). Optimized chemical proteomics assay for kinase inhibitor profiling. J. Proteome Res. *14*, 1574–1586.

Montague, T.G., Cruz, J.M., Gagnon, J.A., Church, G.M., and Valen, E. (2014). CHOPCHOP: a CRISPR/Cas9 and TALEN web tool for genome editing. Nucleic Acids Research *42*, W401–W407.

Murshudov, G.N., Skubák, P., Lebedev, A.A., Pannu, N.S., Steiner, R.A., Nicholls, R.A., Winn, M.D., Long, F., and Vagin, A.A. (2011). REFMAC5 for the refinement of macromolecular crystal structures. Acta Crystallogr. D Biol. Crystallogr. *67*, 355–367.

Ran, F.A., Hsu, P.D., Wright, J., Agarwala, V., Scott, D.A., and Zhang, F. (2013). Genome engineering using the CRISPR-Cas9 system. Nat Protoc *8*, 2281–2308.

Schneider, K.S., Thomas, C.J., and Groß, O. (2013). Inflammasome Activation and Inhibition in Primary Murine Bone Marrow-Derived Cells, and Assays for IL-1α, IL-1β, and Caspase-1. In Methods in Molecular Biology, (Totowa, NJ: Humana Press), pp. 117–135.

Shi, C., Xiong, Z., Chittepu, P., Aldrich, C.C., Ohlfest, J.R., and Ferguson, D.M. (2012). Discovery of Imidazoquinolines with Toll-Like Receptor 7/8 Independent Cytokine Induction. ACS Med Chem Lett *3*, 501–504.

Shi, H., Wang, Y., Li, X., Zhan, X., Tang, M., Fina, M., Su, L., Pratt, D., Bu, C.H., Hildebrand, S., et al. (2016). NLRP3 activation and mitosis are mutually exclusive events coordinated by NEK7, a new inflammasome component. Nat Immunol *17*, 250–258.

Solle, M., Labasi, J., Perregaux, D.G., Stam, E., Petrushova, N., Koller, B.H., Griffiths, R.J., and Gabel, C.A. (2001). Altered cytokine production in mice lacking P2X(7) receptors. J. Biol. Chem. *276*, 125–132.

Tabeta, K., Hoebe, K., Janssen, E.M., Du, X., Georgel, P., Crozat, K., Mudd, S., Mann, N., Sovath, S., Goode, J., et al. (2006). The Unc93b1 mutation 3d disrupts exogenous antigen presentation and signaling via Toll-like receptors 3, 7 and 9. Nat Immunol *7*, 156–164.

Wallace, A.C., Laskowski, R.A., and Thornton, J.M. (1995). Ligplot - a Program to Generate Schematic Diagrams of Protein Ligand Interactions. Protein Eng. *8*, 127–134.

Wang, G.G., Calvo, K.R., Pasillas, M.P., Sykes, D.B., Häcker, H., and Kamps, M.P. (2006). Quantitative production of macrophages or neutrophils ex vivo using conditional Hoxb8. Nature Methods *3*, 287–293.